ON THE BOUNDARY CONDITIONS AT AN OSCILLATING CONTACT LINE: A PHYSICAL/NUMERICAL EXPERIMENTAL PROGRAM

Marc Perlin and William W. Schultz
University of Michigan

ABSTRACT

We will pursue an improved physical understanding and mathematical model for the boundary condition at an oscillating contact line at high Reynolds number begun by Ting & Perlin (1). We expect that the body force is locally unimportant for earth-based systems, and that the local behavior may dominate the mechanics of partially-filled reservoirs in the microgravity environment (Weislogel & Lichter 2).

One important space-based application for this contact-line study is for Faraday-waves. Oscillations in the direction of gravity (or acceleration) can dominate the fluid motion during take-off and reentry with large steady-state accelerations and in orbit, where fluctuations on the order of $10^{-4}g$ occur about a zero mean. Our experience with Faraday waves has shown them to be "cleaner" than those produced by vertical or horizontal oscillation of walls. They are easier to model analytically or computationally, and they do not have strong vortex formation at the bottom of the plate. Hence many, if not most, of the experiments will be performed in this manner. The importance of contact lines in the microgravity environment is well established (Concus, et al. 3; Sigigner & Weislogel 4; Capodanno 5; Kim, et al. 6; Lucassen, et al. 7; Merte, et al. 8).

We will compare high resolution measurements of the velocity field ($10\mu m$ resolution) using particle-tracking and particle-image velocimetry as the fluid/fluid interface is approached from the lower fluid. The spatial gradients in the deviation provide additional means to determine an improved boundary condition and a measure of the slip region, unavailable from the work by Ting & Perlin. Dissipation, the size of the eddy near the contact line, and hysteresis will be measured and compared to linear and nonlinear models of viscous and irrotational but dissipative models.

1 INTRODUCTION AND THE STATE-OF-THE-ART

The contact line is the intersection between two distinct fluids and a solid: here, the fluids are water and air, the solid is glass. The contact angle θ_c is defined as the angle between the tangent to the fluid interface at the contact line and the water-glass interface (see figure 1). Contact-line behavior may be couched as a relationship between the contact angle and the relative (liquid-to-solid) motion of the contact line. "Contact angle" is used in place of "apparent contact angle." (the macroscopic contact angle, Dussan V. 9) To determine and quantify the contact-line behavior, precise measurements of the contact-line position (and thus velocity and acceleration) and dynamic contact angle (*i.e.* contact angle with a moving contact line) must be conducted.

Information regarding the contact line and contact angle in uni-directional viscous flows abounds in the literature. A complete and thorough discussion of static contact angle and dynamic contact angle for uni-directional relative velocities is given by Dussan V. (9). These results are representative for experiments with small Reynolds number, small Weber number, and small Froude number. For these cases, there is no inertial effect from contact-line movement. The relationship shows that the contact angle is a function of the contact-line velocity only, i.e. $\theta_c = f(V_r)$. In figure 2, α_r represents the receding angle defined when $V_r \rightarrow 0^-$ (the contact point moves toward the liquid), α_a represents the advancing angle defined as $V_r \rightarrow 0^+$ (the contact point moves away from the liquid). Because of the hysteresis, the contact-line boundary condition is nonlinear, even for low Reynolds number uni-directional, steady motion.

A difficulty arises in the solution of the viscous flow field — even with a (uni-directionally) moving contact line. Dussan V. & Davis (10) showed that a non-integrable-stress singularity occurs at the contact line if a moving contact line is forced to obey the no-slip boundary condition. A popular model to avoid the singularity that allows the contact point to move along the solid surface was originated by Navier. He postulated that the resistant stress at a fixed solid surface is proportional to the relative velocity or $\beta u = \mu \partial u / \partial n$. Here, β is a constant, u is the velocity parallel to the fixed solid surface, n is the distance normal to the solid surface, and μ is the liquid dynamic viscosity. A terse description of this slip boundary condition is given by Goldstein (11).

As opposed to their uni-directional counterparts, oscillatory contact-line boundaries have not been studied experimentally in a significant way until very recently (1). Oscillatory contact-line boundaries are important in wave and other flow interactions with a solid boundary. Benjamin & Scott (12) and Graham-Eagle (13, 14) investigated waves propagating in a narrow open-channel with pinned-end (fixed contact-line position) edge conditions. Hocking (15)

demonstrated the importance of surface tension effects at a contact line and showed that the damping of gravity-capillary waves at a rigid boundary is mostly due to capillary effects. Several other publications that demonstrate the importance of capillary effects in wave motion and damping include Miles (16, 17, 18); Hocking & Mahdmina (19); Joo, Schultz & Messiter (20); Cocciaro, Faetti & Nobili (21); and Cocciaro, Faetti & Festa (22).

Quantitative information is sparse regarding oscillating contact lines. Based on the relationship given by Dussan V. (9) for uni-directional contact lines, Young & Davis (23) proposed four possible relationships between contact angle and contact-line velocity for an oscillating contact-line boundary: (a) with contact-angle hysteresis; (b) fixed contact line; (c) fixed contact angle; and (d) smooth contact-angle variation (no contact-angle hysteresis). Using these relationships and a force balance at the contact line, they presented a solution to the oscillatory contact-line motion in the creeping-flow limit. They considered small motion of the plate so that the inertial effect is small; therefore, the contact-line behavior is governed by a relationship similar to that of Dussan V. (9). They found that contact-angle hysteresis and steepening of the contact angle with increasing contact-line speed are dissipative effects. Also, they stated that the contact-line motion tends to lag behind the plate motion due to inertia.

Hocking (24) used an oscillatory contact-line boundary condition to calculate the waves generated by a vertically oscillating, vertical plate. Capillary effects were included in his analysis at the contact line. Two approximations originally proposed by Young & Davis (23) to the uni-directional model of Dussan V. (9) were used. Miles (17), addressing the same problem as Hocking, also used a Navier-slip boundary condition along the plate associated with a boundary condition at the contact line. In his analyses, viscosity was included and a non-zero initial free-surface meniscus was also considered in one case. A slip length, l_s (defined as slip velocity divided by shear at the wall), was adopted to replace the no-slip boundary condition along the entire plate. By a phenomenological hypothesis, he posed the slip boundary condition (equivalent to Navier's slip model with $l_s = \mu/\beta$)

$$V - V_{solid} = l_s \frac{\partial V}{\partial n},$$

where V is the vertical velocity along the plate ($\frac{\partial \eta}{\partial t}$ at the contact line). He stated that l_s is a function of position along the plate surface and vanishes at a distance, $l_\nu = \sqrt{2\nu/\omega}$ (the viscous length scale), away from the contact line. That is, the flow obeys the no-slip boundary condition at some distance l_n away from the contact line. For simplicity, he assumed that l_s is constant, but experimental results show this is unrealistic as mentioned by Miles (17).

From the discussion and conclusions of Ting & Perlin, the edge condition at an oscillatory solid boundary (i.e. a trijunction) is shown to be very important, but it is neither fully understood, nor predictable for large contact-line motion. Many theoreticians have adopted some form of the uni-directional model and a slip boundary condition along the solid surface, however, according to measurements by Ting & Perlin, this model is incorrect for large oscillatory (sinusoidal) plate motion. The qualitative behavior of the contact-line movement changes as the amplitude of the plate oscillation changes (figure 3, 4). The mean slip coefficient changes dramatically with oscillation amplitude as shown in figure 5.

Dissipation due to viscosity (and the vortex imaged by Ting & Perlin) and hysteresis are very important, ubiquitous phenomena. We will accurately measure this flow field and compare it directly to numerical results. As an example of the lack of understanding of dissipation in oscillatory flows, many published results present a discussion stating that a one to three order-of-magnitude increase in the viscosity is required to match numerical results with measured dissipation (e.g. Hocking 15 and Henderson & Miles 25). We believe this so-called effective viscosity is the result of contact-line-generated dissipation.

2   OBJECTIVES

The main goal of this research is to provide a physical explanation of oscillatory contact-line behavior, a more accurate boundary model for large-amplitude oscillations, and an attempt to model dissipation in the vicinity of the contact line. The proposed problem clearly requires an energetic, multi-disciplinary approach.

Specific objectives are: (1) to conduct precise measurements of the flow field in the immediate vicinity of the contact line and as a function of position along a vertically oscillating reservoir or upright plate using particle-image-velocimetry techniques; (2) to compare the measured velocity fields with those predicted by the exact analytic solution of Stokes, thus defining the slip region as well as elucidating the effect of the contact line, meniscus, and the interface on the local fluid physics, this by investigating the deviation from the exact solution; (3) to develop a proper boundary condition for the stick-slip motion of the contact-line region (Note that the Ting & Perlin model did not include the effects of acceleration directly.); (4) to develop a numerical code to simulate the flow field using the boundary condition

developed and the viscous equations of motion; and (5) to verify and quantify the accuracy of the boundary conditions developed by comparing the interfacial elevations and flow fields of the measurements with those of the numerics. In the following, we discuss the laboratory facility, experimental techniques, and the experiments; the numerical methods and simulation; the contact-line effects on Faraday waves; and the comparisons to be conducted.

3 LABORATORY FACILITY, EXPERIMENTAL TECHNIQUES, AND EXPERIMENTS

The study will include a synergistic set of physical and numerical experiments as follows: a contact-line model will be developed based upon physical experiments and the deviation of the experiments from the Stokes second problem solution; the newly determined boundary condition used in conjunction with the viscous equations and other boundary conditions will be solved numerically; and a comparison of the physical and numerical wave fields generated will quantify the effectiveness and applicability of the contact-line boundary condition. In addition, the energy dissipation at the contact-line region will be studied, especially with regard to the relatively large vortex discovered by Ting & Perlin.

Using a time series recorded by a high-speed camera of the contact-line region as illuminated by a laser sheet in the presence of dye-laden water, one obtains the position of the plate, the position of the contact line, and the apparent contact angle. Sufficient magnification is achieved with a proper choice of lenses and extension tubes; however, to obtain a detailed velocity field with a large number of velocity vectors still requires resolution available only on film. The relatively poor resolution of the video system was one of the limiting factors on the data of Ting & Perlin (1). These data had insufficient resolution to obtain meaningful accelerations through two differentiations of the plate/contact-line position. Our experience shows that 4"x5" Kodak Tmax 400 film works well for velocimetry with a film resolution on the order of 5 microns. Using the computer to generate the timing sequence, any desired phase of the oscillation can be captured on the film. In addition, a technique developed by Lin & Perlin removes light reflections present in the fluid-fluid interface, thus removing the ambiguity of the interfacial location and recording only those particles actually located in the lower fluid. The region of high shear (as seen by Ting & Perlin) immediately adjacent to the contact-line region will be studied also. From these data, we believe a reasonable boundary condition is achievable. We will have inferred the region (length) of slip through the comparison with the solution of the oscillating plate in a semi-infinite fluid. An improved boundary condition from that used by Ting & Perlin (1) will be formulated, since the acceleration information will now be available.

Experiments to verify the boundary condition will be conducted to determine the interfacial elevation and the particle velocities some distance away from the plate. These data will be used for comparison to the numerical solution of the flow field obtained with the boundary condition developed herein. Thus, the validity and accuracy of the model will be determined. We also intend to evaluate and compare other independent measures of contact angle (Concus, et al. 3; Seebergh & Berg 26; Li, et al. 27; van der Zanden & Chesters 28). Many of these are adapted to the microgravity environment, but may not be applicable for oscillatory flows.

4 NUMERICAL METHODS AND SIMULATION

We will model the flow near the contact line in a 2 × 2 matrix of linear and nonlinear and inviscid and viscous flows. The inviscid model has been developed by Hocking (6), but only for linearized boundary conditions and with a simple contact-angle model that bears no resemblance to figure 2. On the other hand, there have been fully-viscous analyses by several groups (Kafka, et al. 29; Dussan, et al. 30), but for steady, creeping flow.

The flow we wish to model is high Reynolds number. Hocking (15, 24) showed that many of the major features (such as damping) can be retrieved from an inviscid, even irrotational model. This is important as modeling very high Reynolds number flows with a fully-viscous computation is quite daunting. Features such as slip length and the eddy near the contact line must of course be discarded.

We will extend Hocking's analysis to include a more general model for contact-line behavior, namely

$$\theta_c = \theta_c(V_r, \frac{dV_r}{dt}).$$

This model can be made sufficiently general to accommodate the experimental data of figure 3. This data shows that the contact angle versus relative speed has hysteresis itself, as opposed to the "usual" contact angle hysteresis represented by the vertical line in figure 3. A simplification when no contact angle hysteresis exists is possible for periodic motion with a complex λ (Miles 17),

$$V_r = \lambda \frac{\partial \eta}{\partial x},$$

617

at the expense of fitting the data of figure 3 only crudely.

When we model the viscous flow, we again resort first to linearized flow to simplify the problem and make it more amenable to analysis. Now a slip model is required. One important aspect that is not usually studied is that the slip coefficient in the unsteady case must be compatible with the contact angle model to avoid reintroducing a singularity at the origin. Specifically, at the contact line, we have two conditions on slip — a contact-angle condition and a slip condition. For the simplest contact angle relationship we get

$$V_r = \lambda \frac{\partial \eta}{\partial x} = l_s \frac{\partial V_{CL}}{\partial x}.$$

Since $V_{CL} = \partial \eta / \partial t$, this requires that $\lambda = l_s \partial / \partial t$. More complicated compatibility constraints are required for more general contact angle relationships.

In the last year or two of the contract period, we expect to run spectral element computations of modestly high Reynolds numbers. Then the linearized free surface boundary conditions can be relaxed and comparisons of eddy size and strength can be compared with the experiments.

5   CONTACT-LINE EFFECTS ON FARADAY WAVES

We review and discuss some pertinent results from Jiang, et al. (31) as regards contact-line effects on Faraday waves. Specifically, we discuss the competition between viscous effects (tend to decrease frequency) and contact-line effects (tend to increase frequency). The threshold forcing amplitude for the fundamental mode (wavenumber k_i=1) was measured and a stability diagram is presented in figure 6 for three slightly-different fluids and two tank-aspect ratios (AR). Figure 6(a) presents the measurements of water (hollow triangle, AR=10 and hollow diamond, AR=2.61) and mixed water with fluorescein dye (hollow square, AR=10). Also shown is the subharmonic Faraday wave with two wavelengths in the tank (solid triangle, k_i=2, AR=10). Figure 6(b) shows the results for water mixed with Photo Flo 200, volume ratio 100:1 (solid square, AR=2.61 and solid diamond, AR=10). Dimensionless frequency p ($\equiv 4\omega_i^2/\omega_f^2$ where ω_i is the frequency of the excited mode and ω_f is the forcing frequency) and dimensionless forcing amplitude q ($\equiv 2fk_i \tanh k_i h$ where f is the forcing amplitude and h is the water depth) are evaluated based on the inviscid natural frequency ω_i. If p and q lie within the upper and lower solid diagonal lines (unstable region), then subharmonic resonance will occur according to linear theory (Benjamin & Ursell 32); otherwise, the liquid surface is not excited (stable region). The dashed curves represent weakly-nonlinear predictions of Henderson & Miles (24), now denoted by H&M. The hollow circles represent their experiments (with Photo Flo present), shown in figure 6(b).

According to H&M, the viscous natural frequency ω_v should be less than the inviscid natural frequency ω_i, i.e. p_{min}, the p value associated with the minimum of q (q_{min}), should be larger than one. However, our experimental results show an increase in ω_v, not a decrease. As shown in figure 6(a), the p_{min} associated with each set of symbols is less than one, implying that $\omega_v (\equiv \frac{1}{2}\omega_f |_{q_{min}}) > \omega_i$. Benjamin & Scott (13) measured waves propagating in a brimful channel and concluded that the contact-line effect increases the wave celerity (phase speed). By reducing the tank aspect ratio and lessening the relative effect of the contact line by the addition of Photo Flo, we demonstrate this same phenomenon is responsible for our increased ω_v for fixed wavenumber.

The aspect-ratio effect on the frequency is seen in figure 6(a) by comparing measurements in the wider tank (AR=2.61) and those in the narrow tank (AR=10). Due to weaker contact-line effect in the wider tank, ω_v should be and is smaller, corresponding to an increase in p_{min}. Also, since the contact line and wall-boundary layers contribute the most to the dissipation, the effective damping in the wider tank is less owing to the smaller surface-area-to-volume ratio. Therefore q_{min} in the wider tank is smaller.

Figure 6(b) represents our measurements with the mixture of water and Photo Flo. Since the addition of Photo Flo reduces the contact-line effect, p_{min} and q_{min} are relatively more affected by viscous damping and the neutral-stability curve shifts towards H&M's prediction. H&M's theory still overpredicts q on the lower side of the neutral-stability curve and underpredicts ω_v. Their experiments with a water-Photo Flo mixture (hollow symbols) agree with their theory quite well.

6   COMPARISONS

Measurements and numerics will be compared in detail. We will have a "closed-loop" prediction in the sense that our experiments will determine boundary condition along the plate. We will generate numerical solutions with these boundary conditions and finally compare them to the flow field adjacent to the plate to quantify and verify the applicability of our boundary condition.

REFERENCES

1. Ting, C.-L. & Perlin, M. 1995 Boundary conditions in the vicinity of the contact line at a vertically oscillating plate: An experimental investigation. **J. Fluid Mech. 295**, 263-300.
2. Weislogel, M.M. & Lichter, S. 1994 Low gravity capillary flow in a corner. **APS Bulletin 39**, 1871.
3. Concus, P., Finn, R & Zablhi, F. 1992 On canonical cylinder sections for accurate determination of contact angle in microgravity. **Fluid Mechanics Phenomena in Microgravity**, ASME AMD 154.
4. Siginer, D.A. & Weislogel, M.M. (Eds.) 1994 Fluid Mechanics Phenomena in Microgravity. Winter Annual Meeting of ASME. Anaheim, CA, USA.
5. Capodanno, P. 1992 Small oscillations of a liquid in a container of revolution under zero gravity. **Eur J Mech B Fluids 11**, 291-308.
6. Kim, I., Kamotani, Y. & Ostrach, S. 1994 Modeling bubble and drop formation in flowing liquids in microgravity. **AIChE J. 40**, 19-28.
7. Lucassen, J., Lucassen-Reynders, E.H., Prins, A. & Sams, P.J. 1992 Capillary engineering for zero gravity. Critical wetting on axisymmetric solid surfaces. **Langmuir 8**, 3093-3098.
8. Merte, H., Lee, H.S. & Keller, R.B. 1994 Report on Pool Boiling Experiment. Prototype Model Flown on STS-47, Rept. no. UM-MEAM-94-09.
9. Dussan V., E.B. 1979 On the spreading of liquids on solid surfaces: static and dynamic contact lines. **Ann. Rev. Fluid Mech. 11**, 371-400.
10. Dussan V., E.B. & Davis, S.H. 1974 On the motion of a fluid-fluid interface along a solid surface. **J. Fluid Mech. 77**, 71-95.
11. Goldstein, S. 1938 **Modern developments in fluid dynamics**. Vol. 2, Oxford University Press, London, 676.
12. Benjamin, T.B. & Scott, J.C. 1979 Gravity-capillary waves with edge constraints. **J. Fluid Mech. 92**, 241-267.
13. Graham-Eagle, J. 1983 A new method for calculating eigenvalues with application to gravity-capillary waves with edge constraints. **Math. Proc. Camb. Phil. Soc. 94**, 553-564.
14. Graham-Eagle, J. 1984 Gravity-capillary waves with edge constraints. D. Phil. thesis. University of Oxford.
15. Hocking, L.M. 1987 The damping of capillary-gravity waves at a rigid boundary. **J. Fluid Mech. 179**, 253-266.
16. Miles, J.W. 1967 Surface-wave damping in closed basins. **Proc. R. Soc. Lond. A 297**, 459-475.
17. Miles, J.W. 1990 Capillary-viscous forcing of surface waves. **J. Fluid Mech. 219**, 635-646.
18. Miles, J. 1991 Wave motion in a viscous fluid of variable depth: Moving contact line. **J. Fluid Mech. 223**, 47-55.
19. Hocking, L.M. & Mahdmina, D. 1991 Capillary-gravity waves produced by a wavemaker. **J. Fluid Mech. 224**, 217-226.
20. Joo, S.W., Schultz, W.W. & Messiter, A.F. 1990 An analysis of the initial wavemaker problem. **J. Fluid Mech. 214**, 161-183.
21. Cocciaro, B., Faetti, S. & Nobili, M. 1991 Capillary effects on surface gravity waves in a cylindrical container: wetting boundary conditions. **J. Fluid Mech. 231**, 325-343.
22. Cocciaro, B., Faetti, S. & Festa, C. 1993 Experimental investigation of capillary effects on surface gravity waves: non-wetting boundary conditions. **J. Fluid Mech. 246**, 43-66.
23. Young, G.W. & Davis, S.H. 1987 A plate oscillating across a liquid interface: effect of contact angle hysteresis. **J. Fluid Mech. 174**, 327-356.
24. Hocking, L.M. 1987 Waves produced by a vertically oscillating plate. **J. Fluid Mech. 179**, 267-281.
25. Henderson, D.M. & Miles, J. 1990 Single-mode Faraday waves in small cylinders. **J. Fluid Mech. 213**, 95-109.
26. Seebergh, J.E. & Berg, J.C. 1992 Comparison of force and optical techniques for the measurement of dynamic contact angles. **Chem Eng Sci. 47**, 4468-4470.
27. Li, D., Cheng, P. & Neumann, A.W. 1992 Contact angle measurement by axisymmetric drop shape analysis. **Adv. in Colloid and Interface Sci. 39**, 347-382.
28. van Der Zanden, A.J.J. & Chesters, A.K. 1994 Experimental study of the meniscus shape associated with moving liquid-fluid contact lines. **Int. J. Multiphase Flow 20**, 775-787.
29. Kafka, F. & Dussan V. 1979 On the interpretation of dynamic contact lines in capillaries. **J. Fluid Mech. 95**, 539.
30. Dussan V., E.B., Rame, E. & Garoff, S. 1991 On identifying the appropriate boundary conditions at a moving contact line. An experimental investigation. **J. Fluid Mech. 230**, 97-116.
31. Jiang, L., Ting, C.-L., Perlin, M. & Schultz W.W. 1995 Moderate and steep Faraday waves: Instabilities, modulation and temporal asymmetries", submitted to **J. Fluid Mech.**
32. Benjamin, T.B. & Ursell, F. 1954 The stability of the plane free surface of a liquid in vertical periodic motion. **Proc. R. Soc. Lond. A 225**, 505-515.
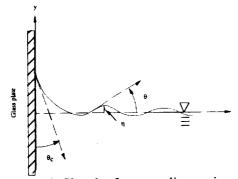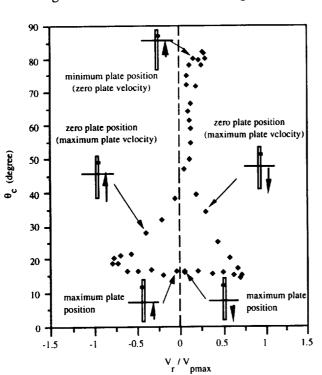
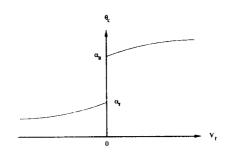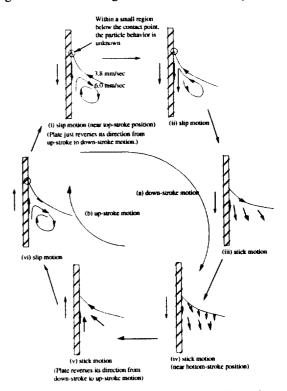Figure 1. Sketch of contact-line region.

Figure 2. Contact angle vs. relative velocity.

Figure 3. Typical graph of the contact angle vs. nondimensional relative velocity.

Figure 4. A pictorial sketch of particle trajectories near the contact line.

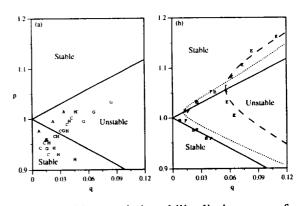Figure 5. Mean slip length versus stroke amplitude.

Figure 6. Subharmonic instability limit curves of Faraday waves for several experiments.

620